Bull. Mater. Sci., Vol. 35, No. 5, October 2012, pp. 847–852. © Indian Academy of Sciences.

Density variation and piezoelectric properties of $Ba(Ti_{1-x}Sn_x)O_3$ ceramics prepared from nanocrystalline powders

A K NATH* **and NIRMALI MEDHI**
Department of Physics, Sri Venkateswara College, University of Delhi, New Delhi 110 021, India

MS received 25 September 2011

Abstract. **Nanocrystalline powders of tin-doped barium titanate with different concentrations of tin have been synthesized by a combination of solid state reaction and high-energy ball milling. The average particle size of the milled powders as determined from TEM analysis was about 5·96 nm. Analysis of all the milled powders using X-ray diffraction method showed single phase perovskite structure. The density variation of the ceramics with sintering temperature has been studied by sintering the samples at different temperatures. Density variation results show that 1350°C is the optimum sintering temperature for tin-doped barium titanate ceramics. SEM micrographs show high density and increasing trend of grain size with increasing content of Sn. The ferroelectricity decreases with increasing concentration of Sn. The electromechanical coupling coefficient also decreases with increasing Sn content corroborating decreasing trend of ferroelectricity. The bipolar strain curves show piezoelectric properties of the prepared ceramics.**

Keywords. **Nanocrystalline powder; high energy ball mill; sintering; ferroelectric.**

1. Introduction

Very high piezoelectric properties have been achieved in a series of lead based perovskite type ceramics (Kuwata *et al* 1982; Park and Shrout 1997). Unfortunately, lead compounds are very toxic and hence from the view point of environmental protection, it is desired that lead-free materials are used as piezoelectric ceramics. In recent years extensive efforts have been done to develop high quality lead-free piezoelectric ceramics to replace toxic lead based materials. Among several groups of lead-free candidates, $BaTiO_3$ is quite promising (Wada *et al* 1999). One of the problems which restrict the application of pure $BaTiO_3$ is that there is a conflict between significant hysteresis in the strain and electric field dependence of the material which leads to difficulty in controlling $BaTiO_3$ based piezoelectric ceramics (Jaffe *et al* 1972; Park *et al* 1999). Barium titanate compositions modified by Sn (Smolenski 1970), Hf (Payne and Tennery 1965), Ce (Hennings *et al* 1994), Y (Jing *et al* 1998), Zr (Ravez and Simon 2001) and other dopants have been studied for dielectric applications.

Barium stannate titanate is a solid solution system of barium titanate and barium stannate. This material was studied by Smolenski (1970) in the early 1970s as a prototype of ferroelectric with different phase transitions. Yasuda *et al* (1996) comprehensively studied the phase transition behaviour, dielectric and ferroelectric properties of barium stannate titanate. However, sintering temperature of barium stannate titanate ceramics is very high and till now no proper study has been done to observe effect of sintering temperature on densification.

The work described here includes synthesis of barium stannate titanate nanopowder by solid state reaction followed by high energy ball milling and studies on the variation of density with sintering temperature to get the best possible sintering temperature for this kind of materials. The piezoelectric and ferroelectric properties of barium stannate titanate ceramics have also been discussed.

2. Experimental

The $Ba(Ti_{1-x}Sn_x)O_3$ nanocrystalline powders were synthesized by a combination of solid state reaction and high-energy ball milling. The raw materials were of high-purity oxide ingredients, $BaCO_3$ (99·9%), TiO_2 (99·9%) and SnO_2 (99·8%). The raw materials were weighed in proportion to the stoichiometric ratio and then thoroughly mixed in an isopropyl alcohol medium using ball mill with zirconia balls. The mixture was dried in an oven and calcined in an alumina crucible at 1050 °C for 4 h in air to yield $Ba(Ti_{1-x}Sn_x)O_3$ where $x = 0{\cdot}025$, 0·045, 0·065, 0·085 and 0·105. The calcined powders were then ball milled using high-energy planetary ball mill (Retsch PM100) at room temperature. The milling was carried out in an isopropyl alcohol medium with agate milling media at a speed of 300 rpm for 25 h. During each high-energy milling, a mass ratio of 1:5 for powder and balls was always maintained. The milling was stopped for 2 min after every 6 min of milling to cool down the system.

*Author for correspondence (anup.tu@gmail.com)

The particle sizes of the milled powders were examined by using TEM (Morgagni 268D). The milled powder was compacted at 2 MPa to form pellets of size 10 mm in diameter and 1 mm in thickness under 2 MPa using polyvinyl alcohol (PVA) as a binder. After burning off PVA, the pellets were sintered at temperatures of 1150°, 1200°, 1250°, 1300°, 1350° and 1400 °C for 4 h in covered alumina crucibles. The bulk density of the sintered specimens was measured using Archimedes principle. The phase identification of the sintered compacts was carried out using an X-ray diffractometer (Philips, PW 3020) with monochromatic CuK_α radiation ($\lambda = 1{\cdot}54178$ Å) over a 2θ angle from 20° to 80°. Scanning electron microscope (SEM/LEO 435VP) was employed to record and analyse the fractured surface morphology of sintered pellets. For electrical measurements, high-purity silver paste was coated on both sides of the flat polished surfaces of the sintered samples and fired at 300 °C for 1 h to form electrodes. The polarization vs electric field (P–E) hysteresis loops of the ceramics were recorded using an automated P–E loop tracer operating at 50 Hz (M/s AR Imagetronics, India). The frequency dependence of dielectric properties was measured with an impedance analyser (Agilent 4294 A). In order to study electrostrictive properties, the field induced strain was measured using a SS50 strain measurement system (Sensor Tec Canada) with a linear voltage differential transducer (LVDT) as displacement sensor and high voltage power supply (4 kV).

3. Results

3.1 *TEM study of nanocrystalline $Ba(Ti_{1-x}Sn_x)O_3$ powders*

As shown in figure 1, TEM micrographs confirm the production of nanocrystalline $Ba(Ti_{1-x}Sn_x)O_3$ powders. A total of 254 particles have been seen in TEM micrograph and size of each particle has been calculated using ImageJ. The particle size varies from a minimum of 3·78 nm to a maximum of 13·03 nm with 4·2 nm size particle mostly occurring. The average particle size calculated using statistical formula comes out to be 5·96 nm.

3.2 *XRD studies*

Figure 2 shows X-ray powder diffraction (XRD) pattern of $Ba(Ti_{1-x}Sn_x)O_3$ ceramics with $x = 0{\cdot}025$, 0·045, 0·065, 0·085 and 0·105 at room temperature obtained after sintering at same conditions of 1350 °C for 4 h. From the XRD patterns, it is evident that all the ceramic samples were crystallized into single phase solid solutions of perovskite structure. It is seen from figure 2 that the structure sensitive (200) peaks shift towards the lower 2θ angles with increasing Sn concentration. This can be attributed to the fact that replacement of Ti^{4+} (ionic radius, 74·5 pm) by Sn^{4+} (ionic radius, 83·0 pm) increases the d spacing (Markovic *et al* 2007). This means that with increasing substitution of Ti by Sn ions leads to unit cell expansion which has been corroborated by shifting of (200) peaks towards lower angles with increasing Sn content. This also indicates that Sn^{4+} is dissolved in the $BaTiO_3$ lattice over a range of compositions we studied.

Applying the Williamson–Hall model (Williamson and Hall 1953), given by

$$\beta \cos\theta = 0{\cdot}9\lambda/D + 4\varepsilon \sin\theta,$$

one can obtain the average crystallite size (D) and microstrain (ε) for a system of interest. Here, β is the full width at half maxima (FWHM) at Bragg's angle (2θ), with λ being the X-ray wavelength of CuK_α ($\lambda = 1{\cdot}54178$ Å). Since the expression represents the equation of a straight line, the lattice strain can be calculated from its slope. Accordingly, the value of microstrain for the Sn-doped ceramics has

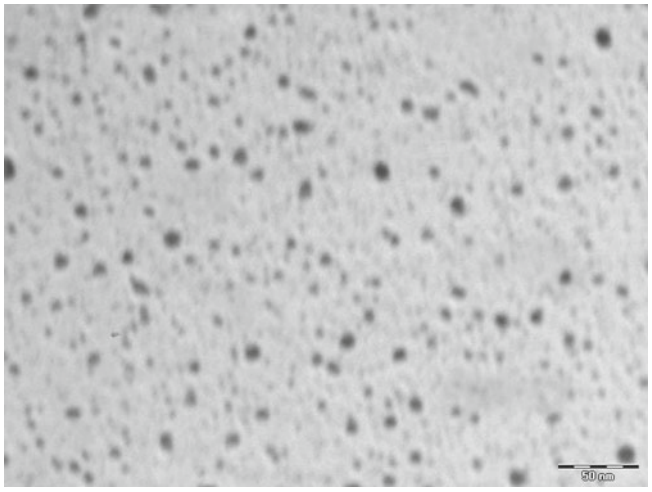

Figure 1. Typical TEM micrograph of milled powder of $Ba(Ti_{1-x}Sn_x)O_3$ ceramic system.

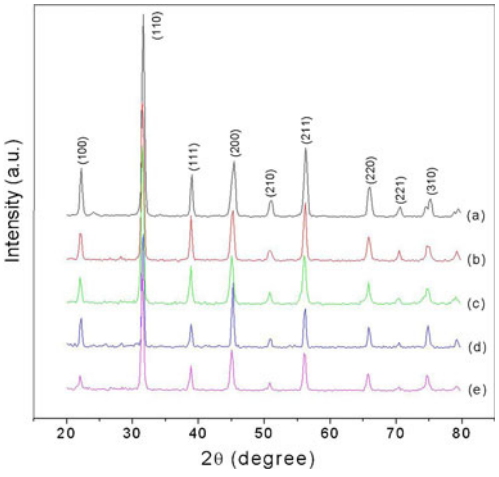

Figure 2. XRD patterns of $Ba(Ti_{1-x}Sn_x)O_3$ ceramics with (**a**) $x = 0{\cdot}025$, (**b**) $x = 0{\cdot}045$, (**c**) $x = 0{\cdot}065$, (**d**) $x = 0{\cdot}085$ and (**e**) $x = 0{\cdot}105$.

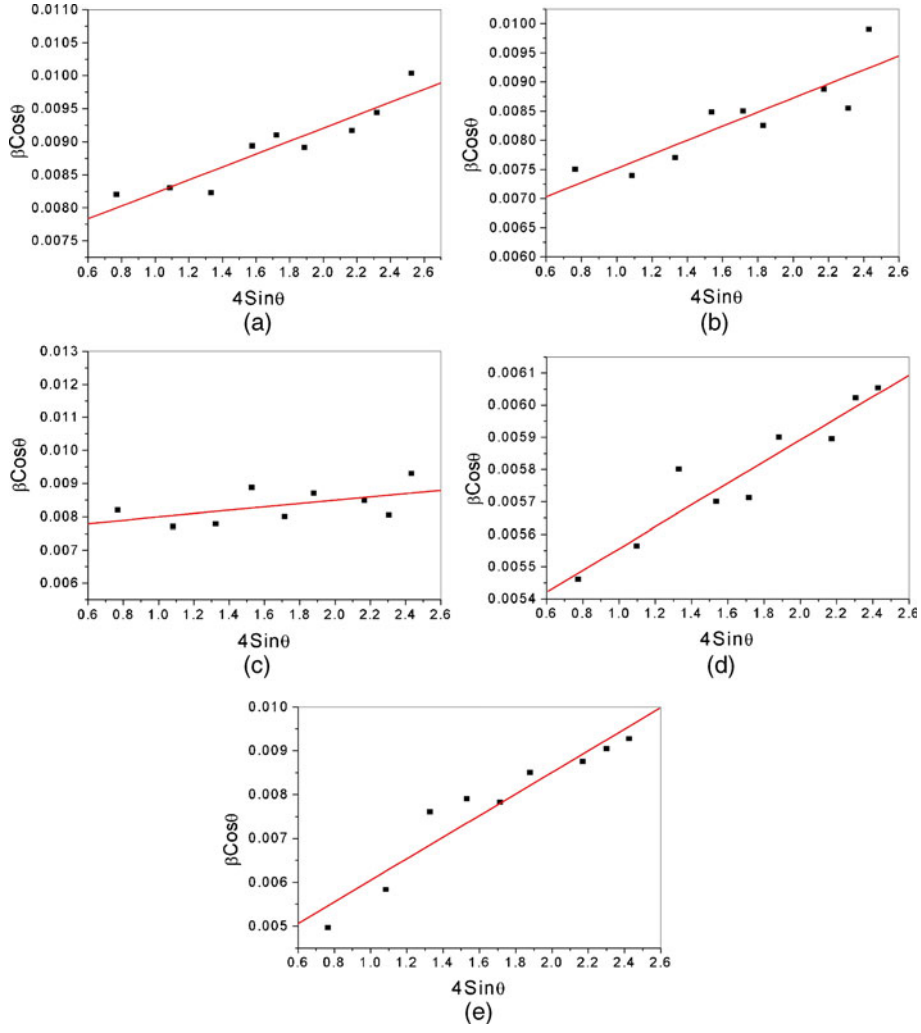

Figure 3. Williamson–Hall plot of $Ba(Ti_{1-x}Sn_x)O_3$ ceramics with (**a**) $x = 0{\cdot}025$, (**b**) $x = 0{\cdot}045$, (**c**) $x = 0{\cdot}065$, (**d**) $x = 0{\cdot}085$ and (**e**) $x = 0{\cdot}105$.

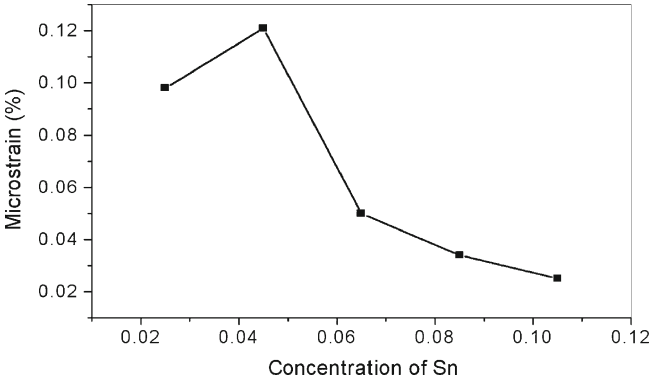

Figure 4. Variation of microstrain with concentration of Sn.

been calculated. The Williamson–Hall plot is shown in figure 3(a–e) and variation of microstrains with Sn concentration is shown in figure 4. The microstrain is maximum for $x = 0{\cdot}045$ and minimum for $x = 0{\cdot}105$. The observed variation in microstrain with concentration (figure 4) can

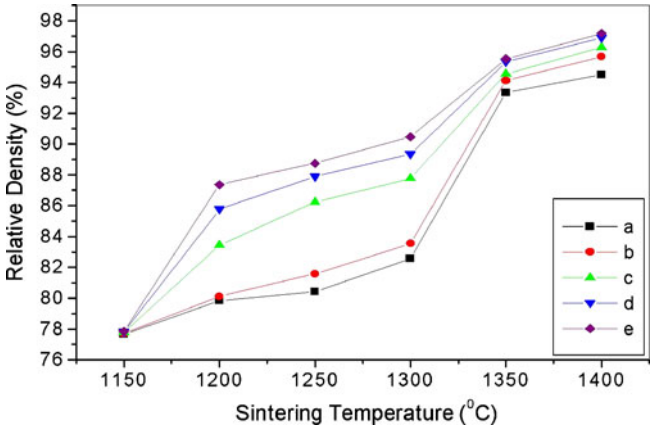

Figure 5. Variation of density with sintering temperature for $Ba(Ti_{1-x}Sn_x)O_3$ ceramics with (**a**) $x = 0{\cdot}025$, (**b**) $x = 0{\cdot}045$, (**c**) $x = 0{\cdot}065$, (**d**) $x = 0{\cdot}085$ and (**e**) $x = 0{\cdot}105$.

be assigned to the fact that due to incorporation of Sn, the Sn^{4+} ions replace the Ti^{4+} ions and accordingly structural modifications take place.

3.3 *Variation of density and shrinkage with sintering temperature*

It is observed that a density of about 77·65–97% of the theoretical value for $Ba(Ti_{1-x}Sn_x)O_3$ has been achieved in the study for different sintering temperatures. Figure 5 shows variation of density with sintering temperature for $Ba(Ti_{1-x}Sn_x)O_3$ ceramics. The density gradually increases with increasing sintering temperature. The maximum density has been obtained for this sample which has been sintered at 1400 °C for 4 h. The change in dimension was gradually increased with sintering temperature from 1150–1250 °C and nearly constant above 1300 °C. The linear shrinkage increased with increasing sintering temperature as shown in figure 6. Hence these results confirmed that the samples were fully sintered at temperatures 1350 °C and 1400 °C kept for 4 h. So, we have an optimum sintering temperature of 1350 °C (for 4 h) for these kinds of lead-free piezoelectric materials. The higher temperature (1400 °C) has been redundant since higher sintering temperature leads to grain growth and reduces certain properties of the ceramics.

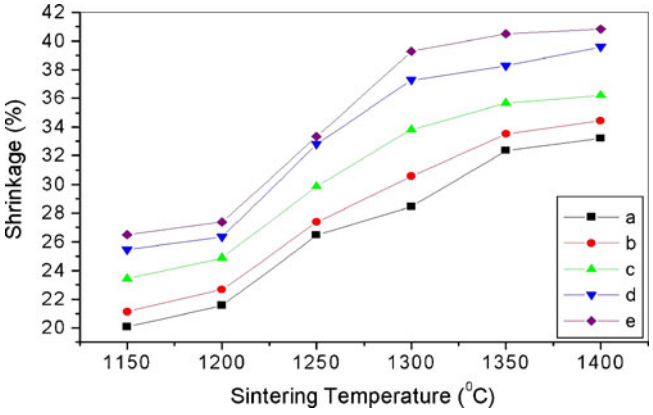

Figure 6. Variation of shrinkage with sintering temperature for $Ba(Ti_{1-x}Sn_x)O_3$ ceramics with (**a**) $x = 0{\cdot}025$, (**b**) $x = 0{\cdot}045$, (**c**) $x = 0{\cdot}065$, (**d**) $x = 0{\cdot}085$ and (**e**) $x = 0{\cdot}105$.

3.4 *Microstructural studies of $Ba(Ti_{1-x}Sn_x)O_3$ ceramics*

Microstructures of the fractured surfaces of $Ba(Ti_{1-x}Sn_x)O_3$ ceramics sintered at 1350°C for 4 h were examined by scanning electron microscope and depicted in figure 7(a, b, c). The grains are not clearly visible in the fractured surfaces indicating that the ceramics are highly dense. Moreover, the micrographs show that the visibility of the grains decreases with increasing content of Sn indicating increasing trend of density which corroborates to the density variation result as shown in figure 5. As seen from the few visible grains, it is observed that the grain size of the ceramics evidently increases with increasing Sn concentration indicating that Sn can promote grain growth of $BaTiO_3$ ceramics. The increase

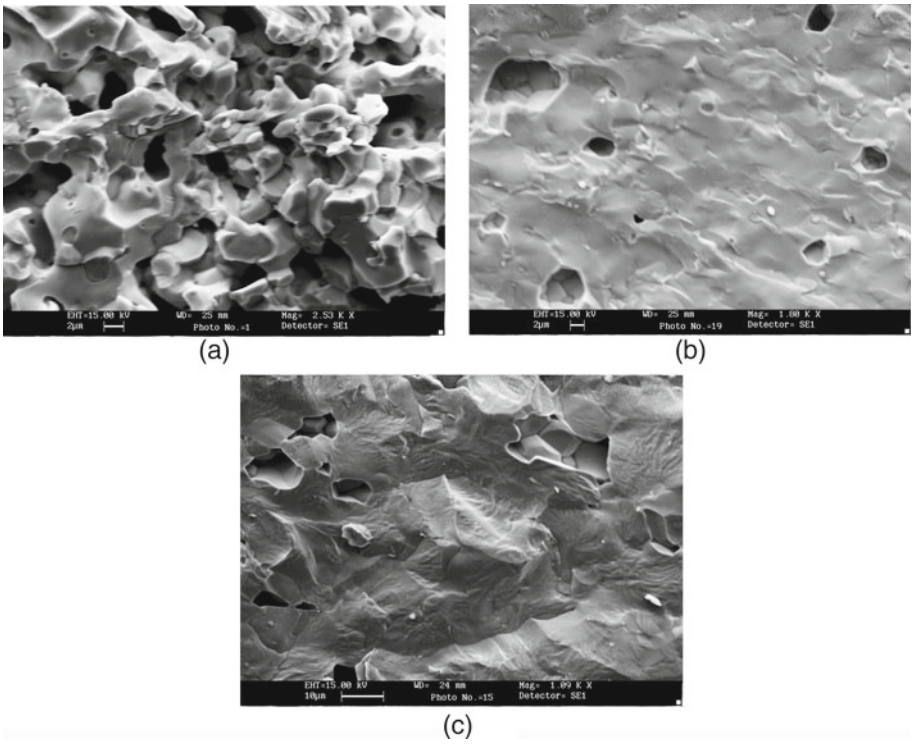

Figure 7. Microstructural patterns of $Ba(Ti_{1-x}Sn_x)O_3$ ceramics with (**a**) $x = 0{\cdot}025$, (**b**) $x = 0{\cdot}045$ and (**c**) $x = 0{\cdot}065$.

in grain size can be explained as follows: The grain growth behaviour is a compromise between the driving force for movement of the grain boundary and retarding forces created by the pores (Kotnala *et al* 2007). Alternatively even if the high energy ball milling can endow with nanoscale powders with high sintering activity, excessive SnO_2 accumulates at the grain boundary and forms oxides with a low melting point that combine with the $BaTiO_3$. The interaction of these two processes leads to grain growth as observed from SEM micrographs.

3.5 *Ferroelectric properties and P–E hysteresis loops*

The polarization hysteresis loops of $Ba(Ti_{1-x}Sn_x)O_3$ samples at room temperature are shown in figure 8(a, b, c, d and e). A clear P–E hysteresis loop can be seen for the ceramics with $x = 0{\cdot}025$, $0{\cdot}045$ and $0{\cdot}065$ signifying that these samples are of ferroelectric nature at room temperature. As the Sn content increases the P–E loops become narrower and practically no loop is formed for $x = 0{\cdot}085$ and $0{\cdot}105$ as these samples fall in paraelectric region.

It has been observed that with increasing concentration of Sn the remnant polarization (P_r) and coercive field (E_c) decreases as shown in figure 9. The narrowing down of hysteresis loops with lower values of P_r and E_c can be correlated to structural changes with changing concentration of tin in agreement with XRD results discussed earlier. Barium stannate titanate is a binary solid solution composed of ferroelectric $BaTiO_3$ and non-ferroelectric barium stannate (Lu *et al* 2004; Wei and Yao 2007). The Sn^{4+} ion replaces the Ti^{4+} ion in $BaTiO_3$ and consequently decreases the ferroelectric property.

3.6 *Variation of piezoelectric constant*

The values of electromechanical coupling coefficients (k_p) of $Ba(Ti_{1-x}Sn_x)O_3$ ceramics for different concentrations of Sn are shown in figure 10. With increasing concentration of Sn, the electromechanical coupling coefficient, k_p, gradually decreases in agreement with the decreasing trend of P_r and E_c values shown in figure 9. For $x = 0{\cdot}025$, the k_p value is 29·1% which deceases to 25·6% for $x = 0{\cdot}065$. The k_p values for $x = 0{\cdot}085$ and $0{\cdot}105$ are zero as the ceramic samples at those compositions are not ferroelectric as evident from ferroelectric properties discussed in the previous section.

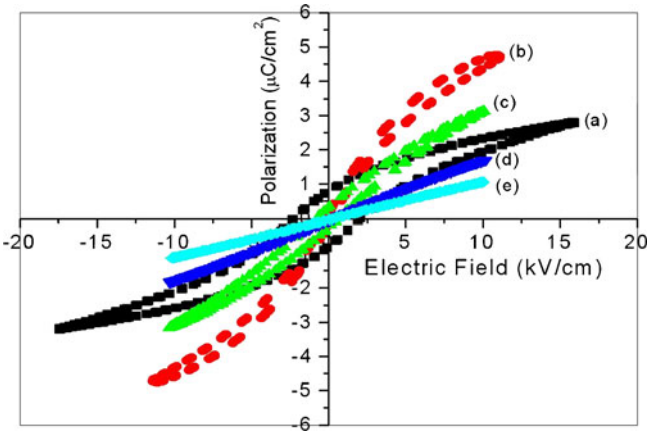

Figure 8. P–E hysteresis curves of $Ba(Ti_{1-x}Sn_x)O_3$ ceramics with (**a**) $x = 0{\cdot}025$, (**b**) $x = 0{\cdot}045$, (**c**) $x = 0{\cdot}065$, (**d**) $x = 0{\cdot}085$ and (**e**) $x = 0{\cdot}105$, measured at 25°C and 50 Hz.

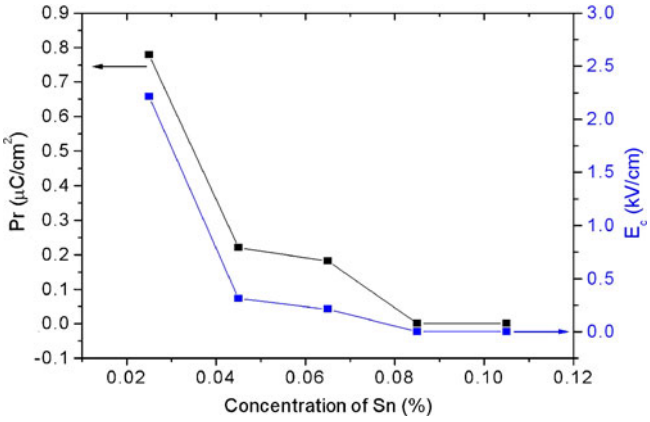

Figure 9. Variation of P_r and E_c with different concentrations of Sn.

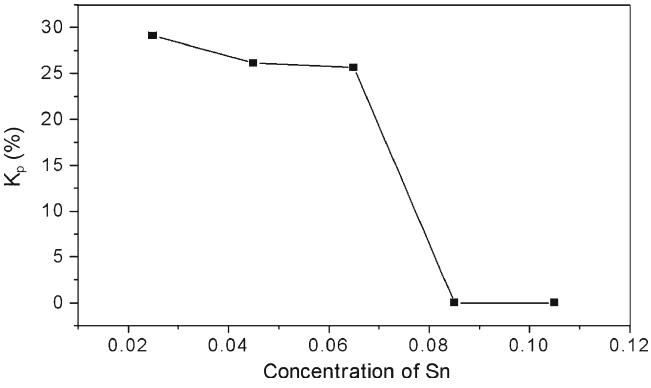

Figure 10. Variation of k_p with varying concentrations of Sn.

3.7 *Electrostrictive strain properties*

The bipolar strain (S) vs electric filed (E) hysteresis loops for $Ba(Ti_{1-x}Sn_x)O_3$ ceramics is shown in figure 11(a, b, c). The hysteretic strain could be associated with the domain reorientation in the samples. It can be seen in figure 11 that the bipolar strain level increases from 0·067% for $x = 0{\cdot}025$ to 0·079% for $x = 0{\cdot}045$. After that for $x = 0{\cdot}065$ the strain again decreases to 0·05%. Compared with other samples, the sample with $x = 0{\cdot}045$ exhibits a reasonably high strain level of 0·079% with proportionately small hysteresis loop area, a property desirable for application in positioning actuators. The observed S vs E profile for $x = 0{\cdot}065$ is due to

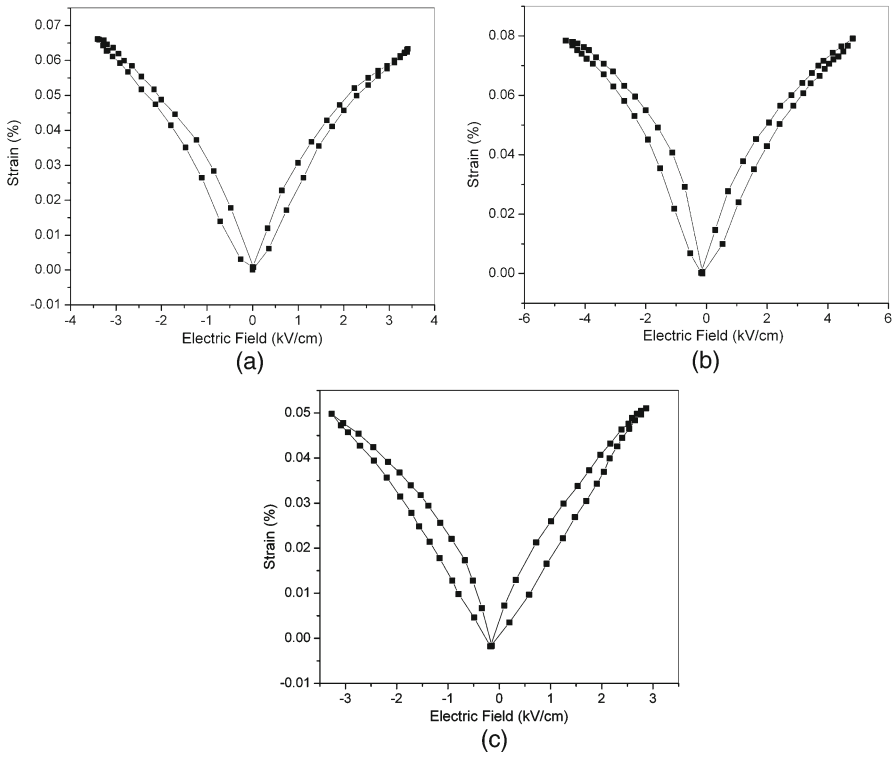

Figure 11. Strain vs electric field curves of $Ba(Ti_{1-x}Sn_x)O_3$ ceramics with (**a**) $x = 0{\cdot}025$, (**b**) $x = 0{\cdot}045$ and (**c**) $x = 0{\cdot}065$.

a mixed state including local polarization contribution originating from the ferroelectric–relaxor behaviour, in addition to the electrostrictive effect of paraelectric state.

4. Conclusions

In this work, we investigated the change in properties of $Ba(Ti_{1-x}Sn_x)O_3$ ceramics with different concentrations of Sn. We were also able to prepare nanosize $Ba(Ti_{1-x}Sn_x)O_3$ powders with a mean particle size of 5·96 nm. The study on the variation of density with sintering temperature confirmed that 1350 °C is the optimum sintering temperature for these kinds of materials. With increasing content of Sn the grain size of $Ba(Ti_{1-x}Sn_x)O_3$ ceramics increases as the excessive SnO_2 accumulates at the grain boundary. It is important to conclude that the ceramics with $x = 0{\cdot}025$, 0·045 and 0·065 showed ferroelectric behaviour with varying values of P_r and E_c. The electromechanical coupling coefficient also decreases with increasing Sn content following the same trend of P_r and E_c. The bipolar strain curves showed that all the three samples which showed ferroelectric behaviour also showed electrostrictive property.

References

Hennings D, Schreinemacher B and Schreinemacher H 1994 *J. Eur. Ceram. Soc.* **13** 81

Jaffe B, Cook W and Jaffe H 1972 *Piezoelectric ceramics* (New York: Academic Press) pp. 47

Jing Z, Ang C, Yu Z, Vilarinho P M and Baptista J L 1998 *J. Appl. Phys.* **84** 983

Kotnala R K, Verma V, Pandey V, Awana V P S, Aloysius R P and Kothari P C 2007 *Solid State Commun.* **143** 527

Kuwata J, Uchino K and Nomura S 1982 *Jpn J. Appl. Phys.* **21** 1298

Lu S G, Xu Z K and Chen H 2004 *Appl. Phys. Lett.* **85** 5319

Markovic S, Mitric M, Cvjeticanin N and Uskokovic D 2007 *J. Eur. Ceram. Soc.* **27** 505

Park S E and Shrout T R 1997 *J. Appl. Phys.* **82** 1804

Park S E, Wada S, Cross L E and Shrout T R 1999 *J. Appl. Phys.* **86** 2746

Payne W H and Tennery V J 1965 *J. Am. Ceram. Soc.* **48** 413

Ravez J and Simon A 2001 *J. Solid State Chem.* **162** 260

Smolenski G A 1970 *J. Phys. Soc. Jpn* **28** 26

Wada S, Suzuki S, Noma T, Susuki T, Osada M, Kakihana M, Park S E, Cross L E and Shrout T R 1999 *Jpn J. Appl. Phys.* **38** 5505

Williamson G K and Hall W H 1953 *Acta Metall.* **1** 22

Wei X and Yao X 2007 *Mater. Sci. Eng.* **B137** 184

Yasuda N, Ohwa H and Asano S H 1996 *Jpn J. Appl. Phys.* **35** 5099